Composites Part B 211 (2021) 108637

Contents lists available at ScienceDirect

Composites Part B

journal homepage: www.elsevier.com/locate/compositesb

Polymer-water interactions and damage detection in polymer matrix composites

Ogheneovo Idolor, Rishabh Debraj Guha, Katherine Berkowitz, Carl Geiger, Matthew Davenport, Landon Grace *

North Carolina State University, USA

ARTICLE INFO

Keywords:
Polymer matrix composites (PMCs)
Laminates
Defects
Non-destructive testing
Near-infrared spectroscopy

ABSTRACT

Polymer matrix composites have a tendency to absorb measurable moisture in nearly all operating environments. This absorbed moisture either becomes bound to the polymer network via secondary bonding interactions or exists as free water with negligible interactions. Damage creates new internal free volume where water molecules can exist in the latter state. This study introduces a novel basis for non-destructive examination in polymer matrix composites which leverages locally-higher concentration of free water in damaged areas. Experiments involved impact-induced sub-surface damage in a laminate prior to moisture exposure. Polymer-water interaction—determining the free or bound state of water—was characterized by near-infrared spectroscopy and microwave-range relative permittivity. Results show a direct correlation between the extent of local damage and higher relative levels of free water at damage sites.

1. Introduction

Over the past two decades, there has been an increase in outdoor applications of polymers and their reinforced composites in electrical, aerospace, marine, oil & gas, and civil infrastructure applications. These applications exploit the high strength-to-weight ratio, corrosion resistance, insulating ability, and desirable dielectric properties that typically drive the adoption of polymer composites [1,2]. However, outdoor applications further complicate efforts to predict long-term performance and service life of polymer composites, an already difficult endeavor even in tightly controlled environmental conditions. Not only are these composites subject to continuous environmental loading such as thermal, moisture, and UV degradation, they are also prone to damage from hail, debris, and other potentially damaging low-velocity impacts which significantly reduce their residual strength [3]. The unpredictability of damage from these sources requires the use of inspection methods that can identify damage in safety-critical structures prior to catastrophic failure. Simple, reliable, and accurate detection of unexpected non-visible damage initiation and progression partially alleviates concerns associated with predicting performance and service life for polymer composite structures operating in complex environments. However, non-destructive detection of damage in polymer composites remains a challenge.

Damage characterization and non-destructive examination (NDE) methods for ascertaining the structural integrity of polymers and composite materials lag behind methods for their metal counterparts in accuracy, flexibility, cost, and simplicity. Methods that have been evaluated for use in polymers and polymer composites include visual inspection, ultrasound, infrared thermography, x-ray radiography, x-ray computed tomography, electromagnetic methods, acoustic emission, acousto-ultrasonic, fiber-optic laser-ultrasound, and shearography, among others [4–10]. These methods have proven moderately successful in characterizing damage but have significant limitations. In general, they lack the ability to capture combined environmental-mechanical effects, characterize damage below the micron scale, or capture chemical changes that may act as precursors to physical damage during the early stages of damage initiation and progression. The ubiquity of moisture in outdoor environments, either through precipitation or humid air, is generally (and correctly) viewed as a contributing factor in performance degradation over time [11–13]. However, the presence of low-levels of moisture in composites that operate in outdoor environments may also enable non-destructive identification of small-scale physical or chemical damage due to the associated change in behavior of nearby water molecules.

Moisture within a polymer network exists in different states based on the nature of its secondary bonding interactions with the polymer

* Corresponding author. Department of Mechanical and Aerospace Engineering 911 Oval Drive, Raleigh, NC 27695, USA.
E-mail address: landon_grace@ncsu.edu (L. Grace).

https://doi.org/10.1016/j.compositesb.2021.108637
Received 20 March 2020; Received in revised form 9 September 2020; Accepted 17 December 2020
Available online 19 January 2021
1359-8368/

network. These states have different effects on the host polymer. For example, plasticization is believed to occur as a result of absorbed moisture that interacts directly with the polymer network via secondary bonding mechanisms [14,15]. This type of water is generally referred to as moisture in the 'bound' state. Furthermore, in polymer composite radomes, water molecules residing in micro-voids that have no secondary bonding interactions with the polymer network are a significant contributor to radar performance degradation due to the associated signal attenuation. Such moisture is regarded as being in the 'free' state [13,16]. These two states of absorbed moisture have been documented extensively by various researchers using gravimetric moisture uptake behavior and numerous characterization tools [1,14,17–21]. Nuclear Magnetic Resonance (NMR) spectroscopy has been applied in studying moisture absorption behavior in polymers, leading to isolation of the effects of free and bound components of absorbed moisture [19,22]. In other studies, molecular dynamics simulations, dielectric relaxation spectroscopy (DRS), differential scanning calorimetry (DSC), and vibrational (infrared) spectroscopy have successfully identified bound and free water as distinct absorbed water states [14,20,23,24]. Musto et al. performed vibrational spectroscopic analysis on epoxy specimens using mid and near-infrared spectroscopy (MIR and NIR). In both cases, contributions from bound and free water were isolated and spectral ranges characteristic of specific types of hydrogen bonding interaction with the water molecule were identified. More importantly, a method to quantitatively estimate the fraction of free and bound water in a polymer specimen by means of NIR spectroscopy was developed [14].

Free and bound water also differ in their response to an applied electromagnetic field. Water, a dipolar molecule, polarizes by rotating in response to an applied electromagnetic field [21,25]. The polarizing tendencies of a material in an electromagnetic field can be described by its dielectric properties. These are usually defined in terms of the complex dielectric constant, comprising the relative permittivity (real part of dielectric constant) and loss tangent (ratio of imaginary to real part of dielectric constant). The ability of a material to polarize in an applied electromagnetic field is closely related to its relative permittivity [26,27], while its relative permittivity is partly dependent on the frequency of the applied electromagnetic field [27,28]. At different frequency ranges, certain mechanisms tend to dominate polarization and hence dielectric contribution as shown in Fig. 1 [29].

Within the 1–10 GHz range (microwave frequency range), the dipolar rotational polarization mechanism dominates dielectric contribution [28,30]. Hence, dipolar molecules such as water are able to rotate with the changing electromagnetic field. The effects of other active polarization mechanisms within the microwave range are minimal, while the larger ionic particles become inactive [28,30]. However, the degree of polarization achieved by a water molecule in a polymer network depends on the nature and extent of rotational restriction resulting from secondary bonding interactions with the polymer

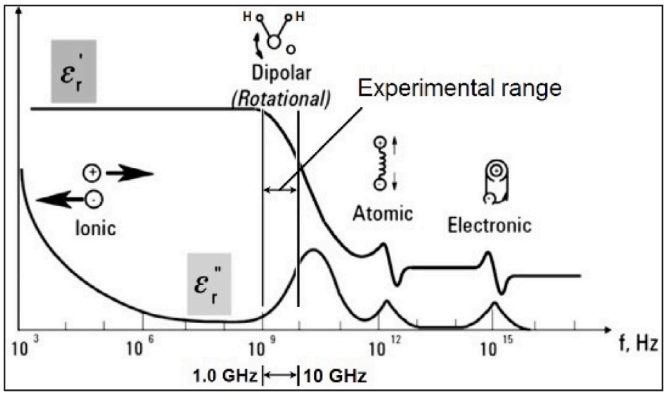

Fig. 1. Changes of Real (ε'_r) and imaginary (ε''_r) parts of complex permittivity with frequency [29].

network [21]. Chemically, water interacts with the polymer network in various ways, including firmly-bound direct hydrogen bonds or less restrictive interactions such as multi-layer, dipole-dipole, or van der Waals forces [17,20]. Physical restrictions also exist due to confinement of water molecules in small cavities such as nano-voids [31,32]. In such scenarios, water is considerably more restricted in its ability to rotate with an oscillating electromagnetic field. Water occupying micro or macro-voids and existing without interactions, however, is free to rotate. Therefore, the relative permittivity of free water within this frequency range is significantly higher (~80) [33], compared to that of firmly bound water (~3) [30], while the relative permittivity of water in the intermediate states (e.g. van der Waals or multi-layer water) will fall between these two extremes [16,34]. Therefore, the bulk relative permittivity of a moisture contaminated polymer matrix composite is not only a function of the relative permittivity of the composite and amount of water present, but also the state of that water. The average state of a water molecule within the polymer network is dependent on the physical and chemical state of the polymer itself, which governs how the water interacts with the polymer. Therefore, changes in the absorbed water state may provide valuable insights regarding the polymer's physical and chemical state via analysis of the changes in the effective relative permittivity.

While near-infrared spectroscopy and microwave-frequency relative permittivity have been applied to polymer matrix composite damage detection in different ways [27,35,36], they have not been based on analysis of water interaction with the polymer. Also, near-infrared spectroscopy has been applied in detection of ultraviolet degradation and thermal damage in polymer matrix composites [35,36], but not in detection of physical damage.

The purpose of this study is to demonstrate the feasibility of a non-destructive evaluation method capable of identifying damage in polymer composites by analyzing the distribution and state of absorbed water molecules. The state and distribution of water is governed in part by the formation of multi-scale voids within the composite resulting from physical damage [37].

2. Methods and materials

2.1. Test materials

An epoxy/glass fiber laminate typical of the aerospace industry was used to fabricate test specimens. The matrix was an epoxy resin, trade name Hexcel F-161. The reinforcement was an 8-harness satin weave glass fabric, style 7781. A 304 × 355 mm laminate was formed from 16 plies of prepreg, ensuring alignment of 0° and 90° directions for all plies. The laminate was cured in a hot press at 386 kPa; it was heated from room temperature at an average rate of 10 °C/minute to 180 °C. The laminate was held at 180 °C for 2 hours, before pressure was released. It was then cooled at an average rate of 2 °C/minute to room temperature. This produced a laminate with an average thickness of 2.9 mm. Individual 54 mm diameter circular test specimens were cut from the larger panel using a diamond-tipped hole saw. This shape and size was necessary in order to meet both NIR spectroscopy and dielectric test specimen geometry requirements. In accordance with ASTM D3171 [38], laminate properties of 5 dried and undamaged specimens were obtained by means of resin burn-off. This was achieved in a high-temperature furnace maintained at 800 °C until elimination of all epoxy residue. Pre and post-burn weight measurements allowed the

Table 1
Average epoxy/glass fiber laminate properties.

Property	Mean (%)	Standard Deviation (%)
Fiber volume fraction	62.3	1.5
Resin volume fraction	32.3	1.1
Void volume fraction	5.4	0.7

estimation of resin, void, and fiber content. Laminate properties are provided in Table 1.

2.2. Sample preparation and impact setup

Circular specimens were dried in a vacuum oven at 65 °C until a stable weight was achieved according to ASTM D5229 [39]. After drying, low velocity out-of-plane impact was applied at the center of the test specimens, with the aim of inducing damage in the form of matrix cracking, fiber/matrix debonding, and delaminations in the laminate [40]. This was achieved using a drop tower equipped with a double column impactor guide mechanism and a crosshead-mounted hemispherical striker tip of radius 9.4 mm, having a total drop-weight of 4.29 kg. The specimen was firmly secured within two steel fixture plates of thickness 3 mm, with circular 35 mm diameter cut-outs. Impacted specimens were positioned concentrically around the cut-outs, ensuring impact at the center of the specimen. The setup was designed to simulate low velocity hail impact on an in-service laminate. Energy levels chosen were expected to generate damage that would not be visibly discernible when paint has been applied on the laminate. The amount of damage induced was varied by adjusting the crosshead height prior to drop, changing its potential energy. Four specimens each for three groups at 0 (undamaged), 3 J, and 5 J impact energies were created.

2.3. Moisture contamination

Gravimetric, dielectric, and NIR data were recorded immediately prior to impact and immediately post-impact. Test specimens were then immersed in deionized water and maintained at 25 °C using a constant-temperature water bath. Specimen weights were measured using a high precision analytical balance. Specimen data was collected periodically over a 3-month period. At each measurement, gravimetric, dielectric (relative permittivity), and NIR absorbance data were recorded. Specimens were first carefully dried using a lint-free cloth and then maintained at ambient conditions for approximately 20 minutes. This eliminated the effects of surface moisture and resulted in a reduction of moisture loss rate from 0.23 mg/minute within the first 5 minutes, to a fairly stable 0.03 mg/minute after 20 minutes; this behavior was consistent and helped minimize uncertainties across measurements.

2.4. Optical microscopy

Micrographs were obtained using a Nikon Eclipse LV150 N optical microscope coupled with a vertically mounted CCD camera. Using a wet diamond-tipped saw, undamaged and 5 J damaged unimmersed specimens were cut along an axis through the impact location as shown in Fig. 2. The cut surfaces were hand polished in several steps using silicon carbide sandpaper of increasingly fine grit, from 400 to 3000. Images were taken at 10x and 20x magnification, while examining the damaged and undamaged specimens.

2.5. Near-infrared spectroscopy

The NIR spectra was obtained from a FOSS 6500 NIR unit equipped with a spinning sample cup module capturing diffuse reflectance from the specimen. The NIR unit produced scans of the infrared spectra from wavelengths of 400–2500 nm (25,000–4000 cm^{-1}) in steps of 2 nm. The wavenumber (cm^{-1}) unit is generally used in spectral analysis and will be adopted in this study. The unit sampled 32 random points at the center of the specimen within the aperture limits of the device,

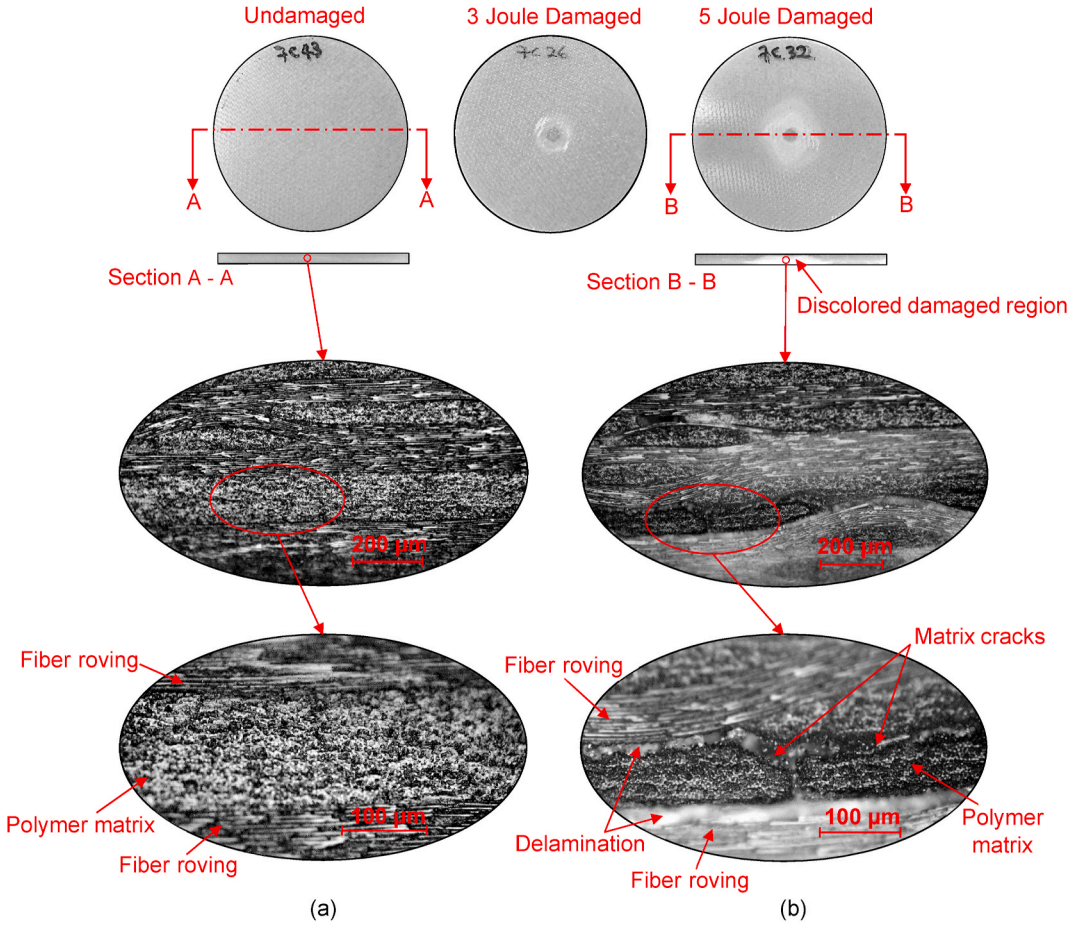

Fig. 2. Sections for micrographs through specimens of (a) undamaged and (b) damaged laminates resulting from a 5 J impact.

producing an average of these as the recorded spectrum for each scan. The specimen was scanned in this way three times, with an average of the three scans taken as the final spectra for each test.

To deconvolute the relevant spectral range into component peaks, a mixed Gaussian-Lorentzian function was adopted to model each peak [14]. Equation (1) gives this mixed function.

$$f(v) = (1-L)\,H\exp\left[-\left(\frac{v-v_o}{w}\right)^2(4\,In\,2)\right] + L\frac{H}{4\left(\frac{v-v_o}{w}\right)^2+1} \quad (1)$$

Where.

v is wavenumber (independent variable)
v_o is peak mean wavenumber
H is peak height
w is full width at half height (FWHH)
L is fraction of Lorentzian character

A model spectra consisting of a combination of the appropriate number of peaks within that spectral range was fitted to the original spectra by applying an algorithm which minimizes the sum of squared error when the model is compared to the measured spectra. This was implemented by using a MATLAB® script to vary the four parameters (v_o, H, w, L) from Equation (1); these determine the shape and position of each peak. The peak combination that provided the closest model fit to the measured spectra was selected. Fig. 3 shows a typical measured spectra within the range of interest, deconvoluted into its 3-peak model spectra.

The area under each peak was then used to calculate the relative concentrations of the various water species according to Equation (2), similar to the methodology adopted in a previous study by Musto et al. [14]. In previous studies, S_0, S_1, and S_2 were designated as different hydrogen bonding states of water, where the subscripts indicate the number of hydrogen atoms in the water molecule participating in external hydrogen bonding [14,17,41]. The approximate locations of the S_0, S_1, and S_2 peaks are shown in Fig. 3.

$$\frac{C_x}{C_{total}} = \frac{A_x}{(A_0 + A_1) + \frac{a_x}{a_2}A_2} \quad (2)$$

Where,

x is number of hydrogen atoms participating in hydrogen bonding (0, 1 or 2)
A_x is peak area for S_x species
C_x is concentration of S_x species
C_{total} is concentration of all species
a_x is integrated absorption coefficients for x species

Equation (2) holds for $x = 0$ and 1 due to similarities in integrated absorption coefficients [14]; however, a similar expression can be derived for $x = 2$.

By using this process, relative concentrations of non-hydrogen bonded water species (S_0), self-associated water-water hydrogen bonded species (S_1), and water-polymer (polar sites) hydrogen bonded species (S_2), were obtained via NIR spectroscopy for all the specimens at different moisture-contaminated conditions [14].

2.6. Microwave relative permittivity measurement

To accurately measure dielectric properties at microwave frequencies, a split post dielectric resonator (SPDR)—fabricated by QWED© of Warsaw, Poland—was coupled with an Agilent programmable vector network analyzer (VNA) as shown in Fig. 4. This setup

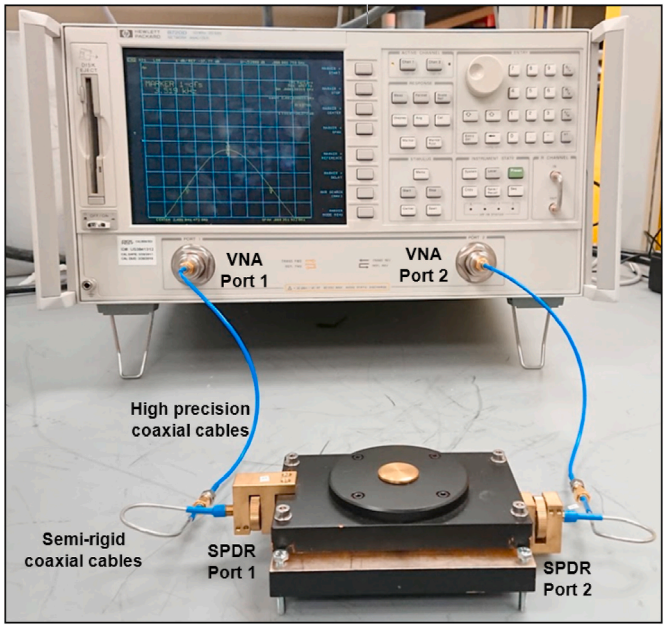

Fig. 4. Split post dielectric resonator (SPDR) coupled to a vector network analyzer (VNA).

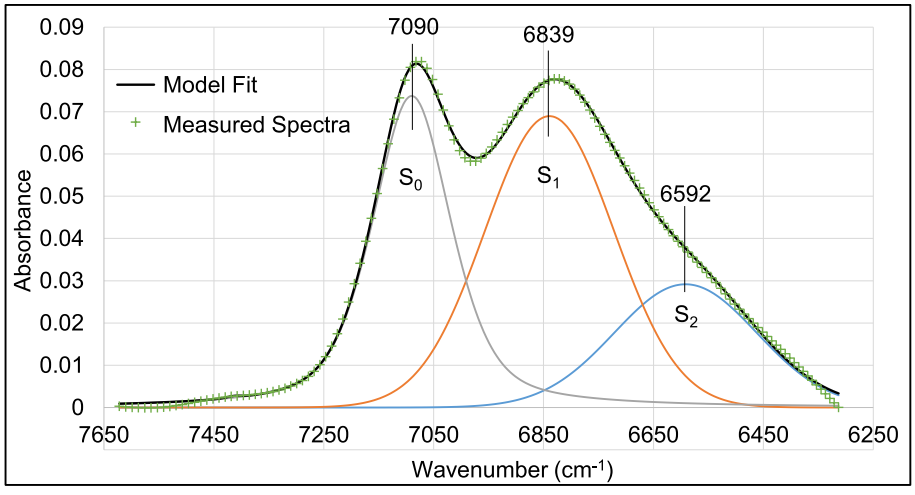

Fig. 3. Typical curve fitting for water spectra of epoxy/glass fiber composite at 0.8% moisture showing 3-peak model within spectral range 6250–7650 cm^{-1}.

enabled measurement of bulk relative permittivity and tracking of small changes in relative permittivity on the order of 10^{-3}. The SPDR utilizes low loss dielectric materials in its construction, allowing the device to resonate at a specific frequency with a very high quality factor (Q-factor). Measurement uncertainty using this setup is 0.3% in relative permittivity, while loss tangent can be measured with resolutions as low as 2×10^{-5} [42]. To calibrate the 2-port system, the scattering parameters S11, S22 and S21 were adjusted. These represent the magnitudes of reflected signal at port 1, reflected signal at port 2, and the signal transmitted from port 1 to port 2 of the SPDR respectively. These were adjusted manually by carefully changing the location of the coupling loops within the resonant cavity. The minimum gain in S11 and S22 were adjusted to be equal prior to adjusting the gain in S21 to −40 dB. For the −3 dB bandwidth calculation, values for resonant frequency and quality factor of the empty resonator were first recorded at 2.48 GHz. Insertion of the specimen under test into the resonant cavity of the SPDR causes a shift in resonant frequency measured using the VNA [43,44]. This resonant frequency shift is used to calculate the real part of relative permittivity (ε'_r) of the specimen according to Equation (3) [42].

$$\varepsilon'_r = 1 + \frac{f_0 - f_s}{h f_0 K_\varepsilon(\varepsilon'_r, h)} \tag{3}$$

Where,

f_0 is resonant frequency of empty SPDR
f_s is resonant frequency with the dielectric specimen inserted
h is sample thickness
K_ε is a function of ε'_r and h, documented in a table unique to each SPDR and provided by the manufacturer

3. Results

3.1. Optical microscopy

Micrograph sections from the undamaged and damaged specimens obtained via the optical microscope described in Section 2.4 are shown in Fig. 2. A typical undamaged specimen viewed by the naked eye has a uniform light green color, while its micrographs show complete and uniform bonding between the fiber roving and polymer matrix. In contrast, unpainted damaged specimens exhibit a white discoloration at and around the impact point. This discoloration was similarly discernible on Section B-B cut through the impact point, with its radius increasing with depth. This is consistent with results reported from previous studies [9]. Micrographs for the damaged specimen show the discoloration to be representative of the damaged area. Within this damaged region, instances of damage-induced new free volume were identified as illustrated in Fig. 2.

3.2. Gravimetric moisture uptake

The average gravimetric moisture uptake data is presented in Fig. 5, where moisture content by weight is plotted against the square root of immersion time. The moisture uptake profiles show a generally linear trend when the early data points of the damaged specimens are excluded. The initially steeper slopes for both damaged specimens likely indicates the preferential diffusion of moisture to occupy voids created by delaminations and matrix cracks within the laminate, both resulting from impact [9,45,46]. The plots also show an increase in the rate of moisture uptake with increasing damage; a result of the increase in potential diffusion pathways in the damaged areas. Gravimetric analysis is a useful tool but is incapable of identifying differences in local moisture concentration compared to bulk water content. Thus, its utility as a damage characterization method is very limited.

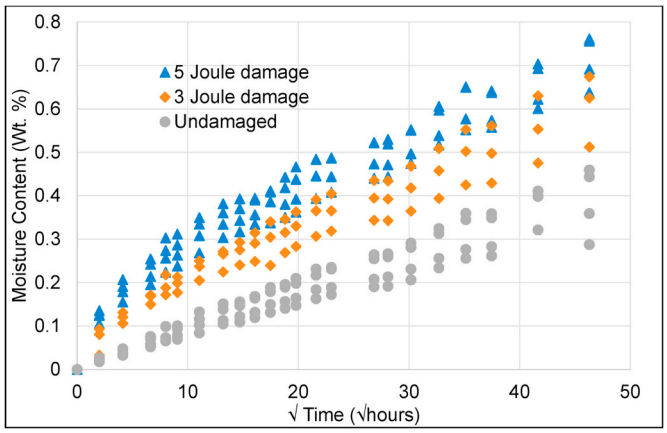

Fig. 5. Plot of moisture content with immersion time.

3.3. Near-infrared spectroscopy

The full NIR spectra obtained is shown in Fig. 6. From this, spectral response for the relevant frequency band (between 6000 and 8000 cm^{-1}, where water can be separated into its free and bound states) was extracted [14].

Analysis of the data involved three major steps: baseline subtraction, subtraction of the initial dry spectra, and fitting a model comprised of a combination of peaks to the obtained spectra [14].

An objective baseline correction algorithm based on a previous study was applied to the spectral data [47]. This involved fitting an n-degree polynomial to the data and then eliminating points that were more than one standard deviation above the fitted line. This process was repeated until the curve converged to the bottom of the peak forming the required baseline. Preliminary results suggested the ideal baseline for this spectral range would be linear [47] (see insert in Fig. 6). Using this algorithm, a linear function fitted to points on both ends of the relevant spectral range was obtained for all conditions; the resulting linear baseline was then subtracted from the spectra. The bounds of the linear function obtained for the 0% moisture (dry) condition formed the basis for the spectral limits adopted for subsequent moisture-contaminated spectra of the tested specimen.

To eliminate the spectral contributions from epoxy and glass fiber constituents of the polymer matrix composite, the baseline-corrected dry spectra was then subtracted from all subsequent baseline-corrected moisture-contaminated spectral conditions [14,48]. Fig. 7 shows spectral curves obtained for increasing levels of moisture contamination.

after baseline correction and dry spectra subtraction. The various spectra shown in Fig. 7 indicate the occurrence of distinct peaks in the vicinity of 7000 cm^{-1}, 6800 cm^{-1}, and a broad peak at 6600 cm^{-1} representing the presence of S_0, S_1, and S_2 species of water molecules [14,17,41].

Knowing the approximate peak positions, the spectra obtained for the various moisture-contaminated conditions were deconvoluted into three peaks; all close to the expected frequencies [14,17,41]. The deconvolution was achieved by minimizing the sum of residuals (error squared). The total residual for each fit was generally of the order 10^{-5} or lower. The summation of these three peaks produced a model that provided a close fit to the measured spectra, as shown in Fig. 3. The area bounded by peaks S_0, S_1, and S_2 were estimated and relative concentration of each species calculated by applying Equation (2).

In estimating relative concentrations of free and bound water, S_0 and S_1 species are designated as free water molecules while S_2 is designated as bound water, consistent with previous studies [14,17,41]. Fig. 8(a) and (b) shows the relative concentration variation of free and bound water with moisture content for an undamged and damaged specimen respectively. In previous studies [14], linear functions provided an

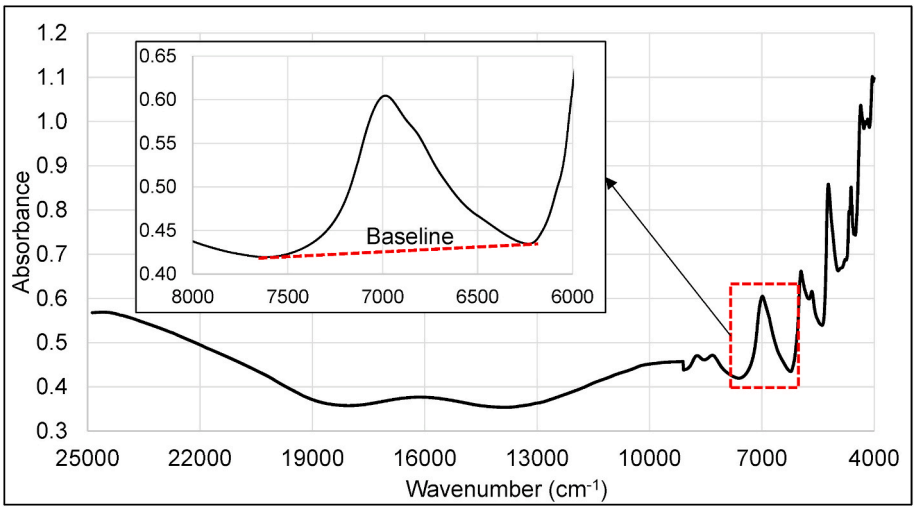

Fig. 6. Typical NIR spectra for moisture contaminated epoxy/glass fiber composite laminate. Insert: Spectral region of interest showing linear baseline to be subtracted.

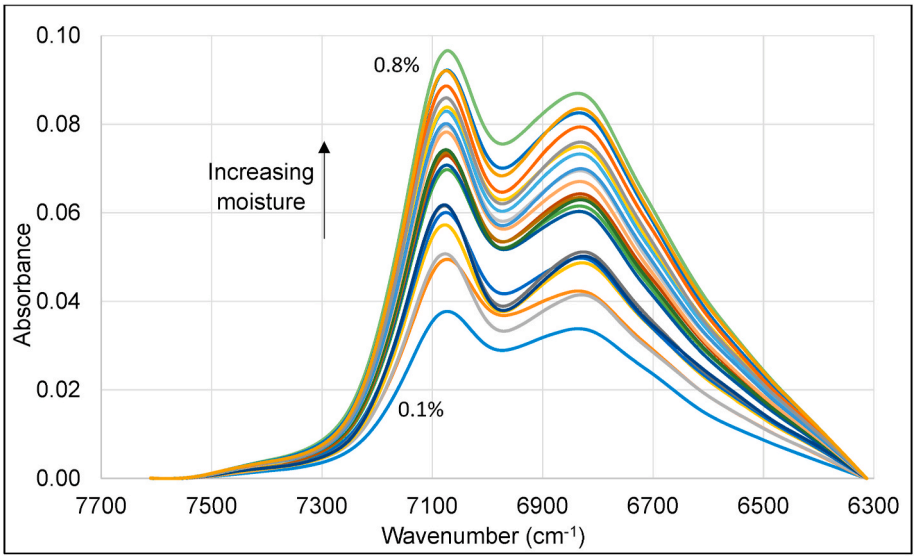

Fig. 7. Typical NIR spectra after baseline correction and subtraction of dry spectra showing effect of increasing levels of moisture contamination from 0.1 to 0.8%.

adequate fit to the free and bound water fraction data. However, to accommodate the damaged specimens in this study—which had a much higher fraction of free water at low moisture content—a more accurate function was needed. Hence, a second-order polynomial fit was adopted. Relative to the linear function, this doubled the correlation coefficient squared (R^2) of the fit to the damaged data, while the fit to the undamaged specimen data remained close to linear even when the higher order function was adopted, consistent with previous studies [14]. Using data from lines of best-fit in Fig. 8 (a) & (b), the ratio of free to bound moisture content—eta (η), is plotted for all three cases (undamaged, 3 J, and 5 J damage) as shown in Fig. 9. Error bars shown indicate twice the standard deviation (±standard deviation); these are obtained when data from all specimens within the same group are considered. In all cases, results show an initially higher proportion of free-to-bound water at low moisture content. This ratio gradually decreases with increasing levels of moisture. Results also show a general increase in η with incresing levels of damage. From this plot a clear distinction can be seen between the proportion of free to bound water in the undamaged specimen compared to the damaged specimens. This is again indicative of free water occupying delaminations and matrix macro and micro-cracks in the damaged specimen (see micrographs for damaged specimen in Fig. 2). The decrease in η suggests a gradual increase in bound water content, indicative of a much slower process of binding water molecules to polar sites within the polymer matrix [49].

3.4. Microwave relative permittivity

The distribution of free and bound water was also investigated through analysis of microwave frequency dielectric properties. The relationship between bulk relative permittivity and immersion time (see Fig. 10) follows a trend similar to the gravimetric uptake curves in Fig. 5. However, relative permittivity is also sensitive to the state of absorbed water in addition to the volume, showing much clearer distinctions between damage levels. This is even more evident when the response in relative permittivity is plotted against moisture content by weight as seen in Fig. 11. This figure clearly demonstrates that relative permittivity is not only a function of the amount of absorbed moisture but also the nature of restriction to dipolar rotation imposed by virtue of its interactions with the polymer matrix (i.e., its state). The change in bulk relative permittivity of the laminate is much more pronounced for the

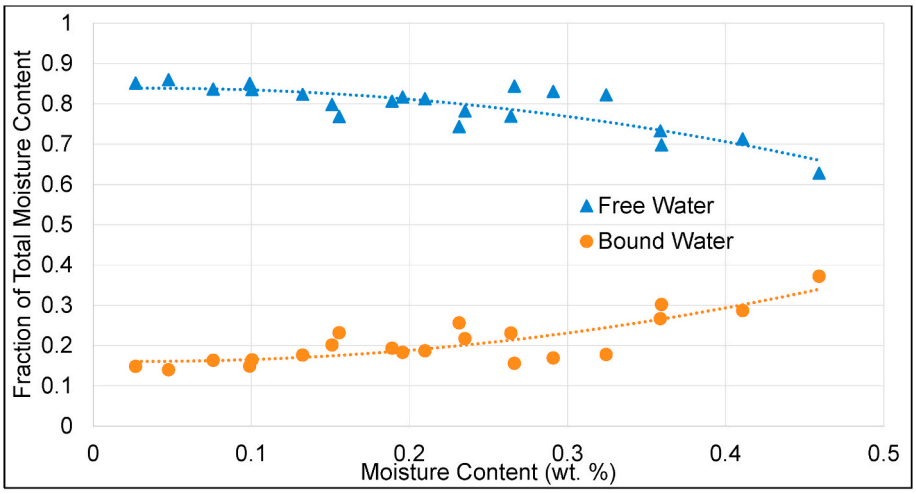

(a)

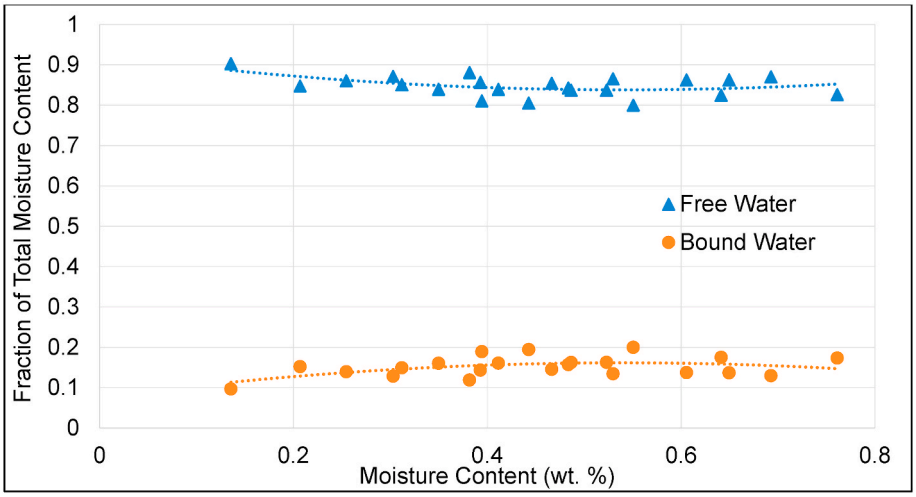

(b)

Fig. 8. Plot showing free and bound water relative concentrations for (a) Undamaged (b) 5 J damaged specimen as a function of total moisture content by weight.

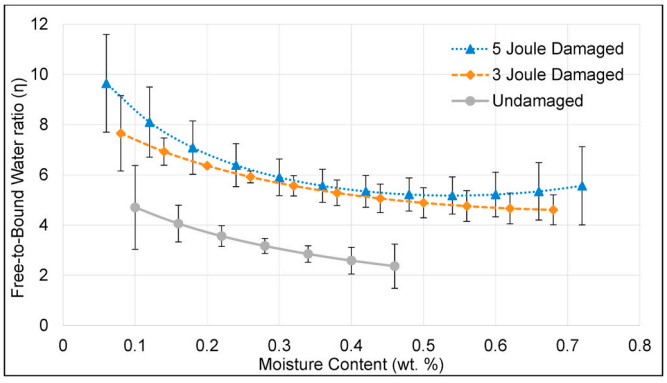

Fig. 9. Plot showing ratio of free to bound water concentration (η) variation with moisture content for epoxy/glass fiber composite when undamaged and damaged at different levels.

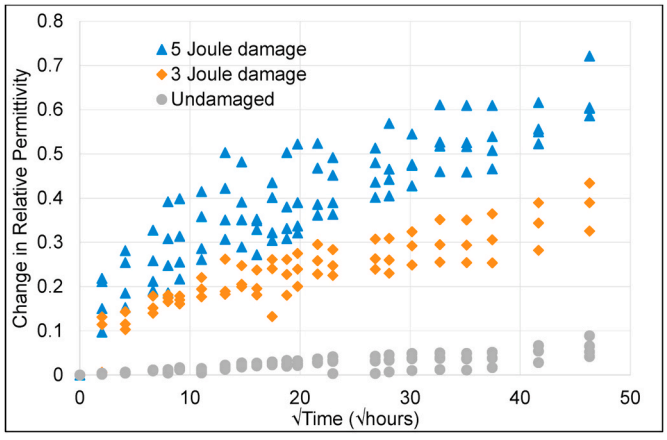

Fig. 10. Plot of change in relative permittivity with immersion time.

damaged specimen, even when the total volume of absorbed water is equivalent between the undamaged and damaged laminates. We can reasonably infer, then, that the higher relative permittivity in damaged specimens at equivalent total water content is the result of higher η. This is consistent with NIR results, and consistent with microscopy results in Fig. 2 that illustrate a higher availability of internal free volume with increased damage.

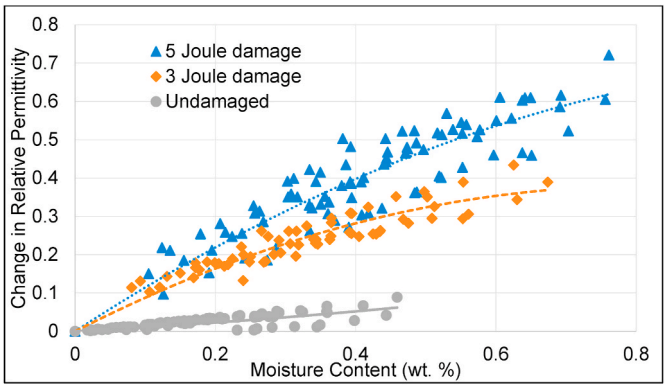

Fig. 11. Plot of change in relative permittivity with moisture content.

4. Discussion

4.1. NIR spectroscopy and microwave relative permittivity comparisons

Data obtained from both NIR spectroscopy and microwave frequency relative permittivity show a similar change in absorbed water state in response to damage. Comparing results from both methods, we can infer that at lower levels of moisture the undamaged specimen contains significantly less free and more bound moisture relative to the damaged specimens. This is evident from its lower η (see Fig. 9) and the significantly slower rise in relative permittivity for the undamaged specimen relative to the damaged specimens at lower moisture levels (see Fig. 11).

This trend changes with increasing moisture, showing a gradual decline in η as well as a less steep increase in relative permittivity. This implies a higher concentration of moisture in the bound state relative to the free state with increasing moisture content. This also implies an initial preferential diffusion of moisture in the free state to occupy macro and micro-voids created as a result of laminate damage. When the influence of dynamic moisture concentration profiles on unsaturated polymer matrix composites is considered, the same conclusions are reached. Studies that investigated the dynamic moisture concentration profile in polymer matrix composites, suggest a much higher concentration of moisture closer to the edges than at the center of the specimen during the early stages of moisture uptake [50]. Since the damaged region is at the center, water would rapidly migrate to the voids in the damaged region through a network of microcracks and exist in the free state; hence, resulting in higher η. At saturated moisture levels, similar logic would apply resulting in higher levels of bound water overall but still a locally higher level of free water at the damaged regions.

Both methods also showed sensitivities to the magnitude of damage induced in the laminates. Although NIR spectroscopy generally showed higher η for increasing levels of damage as seen in Fig. 9, the distinction between 3 and 5 J damage was not as pronounced as in the microwave relative permittivity data. This limitation in sensitivity to damage magnitude when applying NIR spectroscopy could result from a number of factors such as the small difference in damage level (3 J vs 5 J), the non-uniform damage area, and the limited size of sampling area (aperture size of approx. 20 mm diameter) tested relative to the much larger damage-affected region. Hence, NIR absorbance due to moisture at a highly damaged local area may be similar or even higher for a 3 J damaged specimen compared to absorbance at a less damaged local region in a 5 J damaged specimen. This was much less of a problem with the dielectric data as the 2.48 GHz SPDR had an apperture size of over 50 mm diameter. Hence, an electric field was being applied to over 90% of the specimen area during each measurement. This meant that virtually all of the damage-affected regions contributed to the increase in relative permittivity, thereby capturing the overall effect of 3 J or 5 J damage and giving a more accurate represenation of the damage magnitude. This clear distinction in relative permitttivity between 3 and 5 J damage specimen is shown in Figs. 10 and 11. However, this would be less of a limitation in practical applications where spatial variations of η or relative permittivity over a wide area would be collected and used to create a damage map of the laminate [44]. In such an application, a smaller apperture such as in NIR spectroscopy may provide more accurate results and probably better damage mapping and identification resolutions.

4.2. Feasibility and limitations of water interaction-enabled non-destructive examination (WINDE)

The use of water as a type of 'imaging agent' for NDE can be implemented in a variety of characterization techniques that are sensitive to the free and bound state of water [14,21,22,51]. The characterization techniques utilized in this study have demonstrated this possibility. However, limitations of each technique may impede its application to specific conditions. In the case of microwave dielectric properties, a theoretical limitation may result from its insensitivity to free water that is physically bound. This may limit its detection to flaw sizes above length scales at which the chemically-free water begin to act as bound water due to physical confinement [32,34]. Another limitation of applying the microwave-frequency dielectric properties as a characterization method is its limitation to only non-conductive materials. Unlike non-conductive dielectric materials that retain their outer shell valence electrons when an electric field is applied and are restricted to polarization only, conductors allow their outer shell valence electrons to migrate throughout the material, hence invalidating the polarization concept [52]. Similarly, characterization depth limitations exist for NIR spectroscopy in diffuse reflectance mode. Sensitivity of the technique may be limited when damage is beyond the maximum penetration depth for infrared radiation in the medium [53], or when strongly absorbing materials such as carbon fiber is used as polymer reinforcement [54].

Additionally, the sensitivity of the method is a function of the total moisture content as well as the relative amount of free and bound water in the system. The total moisture content of a polymer composite changes with the humidity level of its surroundings based on moisture concentration differences and diffusion laws. However, there is also a higher tendency to lose and gain free water compared to bound water, which requires a higher activation energy due to hydrogen bonding to polar sites [22,55]. This behavior may cause a decrease in the amount of free water residing in the damaged region, thereby affecting sensitivity to damage. Initial sensitivity immediately after damage may also be affected by dependence on the natural process of moisture diffusion. The time required before the method can detect damage may range from a few hours post-impact to a few days. This would depend on the matrix polarity [56], humidity of the operating environment, and the amount of moisture absorbed in the material before damage occurs [44]. Further investigations could examine the influence humidity level of the operating environment would have on sensitivity and the delay in damage detection.

For safety critical systems, early detection of damage at the initiation stage plays an important role in estimation of the remaining useful life of a component. This early stage of composite damage initiation involve matrix micro-cracking. However, detection of micro-cracks at such early stages of damage currently poses a challenge for existing composite NDE methods [4,9]. Of the well-established methods, few can provide useful details about the state of the materials at and below the micro-scale; acoustic emission, x-ray radiography & computed tomography, non-linear acoustics, and resistivity have the capacity to detect matrix micro-cracks but not without limitations [4,9]. These limitations have been reported in previous studies and generally include safety concerns and non-suitability for field use (in the case of x-rays), inability to provide flaw size information (acoustics), and requirements for multiple electrodes or limitation to conductive materials (resistivity). The proposed method of analyzing the nature of moisture interaction may provide a suitable way to characterize these micro-cracks without the

highlighted limitations.

5. Conclusion

This study investigated the possibility of leveraging the effects of damage on the nature of polymer-water interaction in the detection of local damage within a polymer matrix composite. Barely visible damage was induced in 16-ply epoxy/glass fiber laminate specimens via impact at 0 (undamaged), 3 J, and 5 J energy levels before moisture exposure. Gravimetric, near-infrared (NIR) absorption and microwave-frequency dielectric properties were measured periodically within a 3-month period during which the specimens were exposed to moisture. Analysis of results obtained via gravimetric moisture uptake indicate the possibility of detecting the presence of damage within a composite structure but with limited information on spatial distribution or location of damage. Results from NIR spectroscopy indicate higher amounts of free water relative to bound water in damaged specimen, showing as much as a 2-fold higher free-to-bound water ratio in 5 J damaged specimen when compared to an undamaged specimen. Similarly, results from microwave dielectric analysis show as much as an 8-fold higher change in relative permittivity for the same level of damage compared to an undamaged specimen and within the same range of moisture content. Both characterization methods also indicate sensitivity to the magnitude of damage, with microwave relative permittivity showing better differentiation between 3 and 5 J damage, likely due to the larger aperture size of the split post dielectric resonator. These results indicate a higher proportion of bound water in the undamaged laminate, while free water preferentially migrates to voids created by matrix cracking and delaminations within damaged regions. Hence, the study has shown that analysis of polymer-water interactions within a polymer matrix may provide an opportunity to accurately detect low levels of damage and estimate its magnitude and location. Leveraging such molecular-level interactions within the polymer matrix may enable detection of damage at length scales beyond current polymer matrix composite non-destructive examination methods. It may also enable characterization of combined physical-chemical damage modes such as hygrothermal loading and physical damage.

Credit author statement

Ogheneovo Idolor: Conceptualization, Methodology, Investigation, Software, Data Curation, Visualization, Formal analysis, Writing- Original draft.**Rishabh Debraj Guha**: Conceptualization, Writing- Review and Editing. **Katherine Berkowitz:** Investigation. **Carl Geiger:** Data Curation, Software. **Matthew Davenport:** Investigation. **Landon Grace:** Conceptualization, Supervision, Project Administration, Funding acquisition, Resources, Writing – Review and Editing

Declaration of competing interest

The authors declare that they have no known competing financial interests or personal relationships that could have appeared to influence the work reported in this paper.

Acknowledgments

The support of William Woodbridge and Romeo Jump of the College of Natural Resources at North Carolina State University is appreciated for assistance with obtaining near-infrared spectroscopy data. Bassey Enebong Bassey is also appreciated for aiding with graphical visualizations during the project.

Appendix A. Supplementary data

Supplementary data to this article can be found online at https://doi.org/10.1016/j.compositesb.2021.108637.

Funding

This work was supported by the National Science Foundation [Grant No. CMMI-175482].

References

[1] Krauklis AE, Gagani AI, Echtermeyer AT. Near-infrared spectroscopic method for monitoring water content in epoxy resins and fiber-reinforced composites. Materials 2018;11. https://doi.org/10.3390/ma11040586.
[2] Neşer G. Polymer based composites in marine use: history and future trends. Procedia Eng 2017;194:19–24. https://doi.org/10.1016/j.proeng.2017.08.111.
[3] Caputo F, De Luca A, Lamanna G, Lopresto V, Riccio A. Numerical investigation of onset and evolution of LVI damages in Carbon-Epoxy plates. Compos B Eng 2015; 68:385–91. https://doi.org/10.1016/j.compositesb.2014.09.009.
[4] Duchene P, Chaki S, Ayadi A, Krawczak P. A review of non-destructive techniques used for mechanical damage assessment in polymer composites. J Mater Sci 2018; 53:7915–38. https://doi.org/10.1007/s10853-018-2045-6.
[5] Gholizadeh S. A review of non-destructive testing methods of composite materials. Procedia Struct Integr 2016;1:50–7. https://doi.org/10.1016/j.prostr.2016.02.008.
[6] Jolly M, Prabhakar A, Sturzu B, Hollstein K, Singh R, Thomas S, et al. Review of non-destructive testing (NDT) techniques and their applicability to thick walled composites. Procedia CIRP 2015;38:129–36. https://doi.org/10.1016/j.procir.2015.07.043.
[7] Dattoma V, Panella F, Pirinu A, Saponaro A. Advanced NDT methods and data processing on industrial CFRP components. Appl Sci 2019;9:393. https://doi.org/10.3390/app9030393.
[8] Pagliarulo V, Rocco A, Langella A, Riccio A, Ferraro P, Antonucci V, et al. Impact damage investigation on composite laminates: comparison among different NDT methods and numerical simulation. Meas Sci Technol 2015;26. https://doi.org/10.1088/0957-0233/26/8/085603.
[9] Bossi RH, Giurgiutiu V. Nondestructive testing of damage in aerospace composites. Polym Compos Aerosp Ind 2014;413–48. https://doi.org/10.1016/B978-0-85709-523-7.00015-3.
[10] Pelivanov I, Buma T, Xia J, Wei CW, O'Donnell M. NDT of fiber-reinforced composites with a new fiber-optic pump-probe laser-ultrasound system. Photoacoustics 2014;2:63–74. https://doi.org/10.1016/j.pacs.2014.01.001.
[11] Kumar Gupta S, Hojjati M. Microcrack detection in composite laminates at early stage of thermal cycling using moisture/freeze/dry cycle. Int J Compos Mater 2019;2019:7–15. https://doi.org/10.5923/j.cmaterials.20190901.02.
[12] Zafar A, Bertocco F, Schjødt-Thomsen J, Rauhe JC. Investigation of the long term effects of moisture on carbon fibre and epoxy matrix composites. Compos Sci Technol 2012;72:656–66. https://doi.org/10.1016/j.compscitech.2012.01.010.
[13] Berkowitz K, Idolor O, Pankow M, Grace L. Combined effects of impact damage and moisture exposure on composite radome dielectric properties. Int. SAMPE Tech. Conf. 2018;2018– May.
[14] Musto P, Ragosta G, Mascia L. Vibrational spectroscopy evidence for the dual nature of water sorbed into epoxy resins. Chem Mater 2000;12:1331–41. https://doi.org/10.1021/cm9906809.
[15] Zhou J, Lucas JP. Hygrothermal effects of epoxy resin. Part II: variations of glass transition temperature. Polymer 1999;40:5513–22. https://doi.org/10.1016/S0032-3861(98)00791-5.
[16] Grace LR. The effect of moisture contamination on the relative permittivity of polymeric composite radar-protecting structures at X-band. Compos Struct 2015; 128:305–12. https://doi.org/10.1016/j.compstruct.2015.03.070.
[17] Takeshita Y, Becker E, Sakata S, Miwa T, Sawada T. States of water absorbed in water-borne urethane/epoxy coatings. Polymers 2014;55:2505–13. https://doi.org/10.1016/j.polymer.2014.03.027.
[18] Herrera-Gómez A, Velázquez-Cruz G, Martín-Polo MO. Analysis of the water bound to a polymer matrix by infrared spectroscopy. J Appl Phys 2001;89:5431–7. https://doi.org/10.1063/1.1365427.
[19] Popineau S, Rondeau-Mouro C, Sulpice-Gaillet C, Shanahan MER. Free/bound water absorption in an epoxy adhesive. Polymer 2005;46:10733–40. https://doi.org/10.1016/j.polymer.2005.09.008.
[20] Mijović J, Zhang H. Molecular dynamics simulation study of motions and interactions of water in a polymer network. J Phys Chem B 2004;108:2557–63. https://doi.org/10.1021/jp036181j.
[21] Garden L, Pethrick RA. A dielectric study of water uptake in epoxy resin systems. J Appl Polym Sci 2017;134:1–12. https://doi.org/10.1002/app.44717.
[22] Zhou J, Lucas JP. Hygrothermal effects of epoxy resin. Part I: the nature of water in epoxy. Polymer 1999;40:5505–12. https://doi.org/10.1016/S0032-3861(98)00790-3.
[23] Mijović J, Zhang H. Local dynamics and molecular origin of polymer network-water interactions as studied by broadband dielectric relaxation spectroscopy, FTIR, and molecular simulations. Macromolecules 2003;36:1279–88. https://doi.org/10.1021/ma021568q.
[24] Debraj Guha R, Idolor O, Grace L. An atomistic simulation study investigating the effect of varying network structure and polarity in a moisture contaminated epoxy network. https://doi.org/10.1016/j.commatsci.2020.109683; 2020.
[25] Hallikainen MT, Ulaby FT, Dobson MC, El-Rayes MA, Wu L-K. Microwave dielectric behavior of wet soil - Part I: emprical models and experimental observations. IEEE Trans Geosci Rem Sens 1985;23:25–34. https://doi.org/10.1109/TGRS.1985.289497.

[26] Hougham G, Tesoro G, Viehbeck A, Chapple-Sokol JD. Polarization effects of fluorine on the relative permittivity in polyimides. Macromolecules 1994;27:5964–71. https://doi.org/10.1021/ma00099a006.
[27] Zoughi R. Microwave non-destructive testing and evaluation. Dordrecht; Boston. Kluwer Academic Publishers, [2000]; 2000.
[28] Giannoukos G, Min M, Rang T. Relative complex permittivity and its dependence on frequency. World J Eng 2017;14:532–7. https://doi.org/10.1108/WJE-01-2017-0007.
[29] Levy RA, Collier RJ. Principles of solid state physics. Phys Today 1969;22:75–6. https://doi.org/10.1063/1.3035636.
[30] Komarov V, Wang S, Tang J. Permittivity and measurements. Encycl RF Microw Eng; 2005. p. 3693–711. https://doi.org/10.1002/0471654507.eme308.
[31] De Luca S, Kannam SK, Todd BD, Frascoli F, Hansen JS, Daivis PJ. Effects of confinement on the dielectric response of water extends up to mesoscale dimensions. Langmuir 2016;32:4765–73. https://doi.org/10.1021/acs.langmuir.6b00791.
[32] Senapati S, Chandra A. Dielectric constant of water confined in a nanocavity. J Phys Chem B 2001;105:5106–9. https://doi.org/10.1021/jp011058i.
[33] Fernández DP, Mulev Y, Goodwin ARH, Sengers JMHL. A database for the static dielectric constant of water and steam. J Phys Chem Ref Data 1995;24:33–70. https://doi.org/10.1063/1.555977.
[34] Boyarskii DA, Tikhonov VV, Komarova NY. Model of dielectric constant of bound water in soil for applications of microwave remote sensing. Prog Electromagn Res 2002;35:251–69. https://doi.org/10.2528/PIER01042403.
[35] Kumar BG, Singh RP, Nakamura T. Degradation of carbon fiber-reinforced epoxy composites by ultraviolet radiation and condensation. J Compos Mater 2002;36:2713–33. https://doi.org/10.1106/002199802028682.
[36] Toivola R, Afkhami F, Baker S, McClure J, Flinn BD. Detection of incipient thermal damage in carbon fiber-bismaleimide composites using hand-held FTIR. Polym Test 2018;69:490–8. https://doi.org/10.1016/j.polymertesting.2018.05.036.
[37] Claus J, Santos RAM, Gorbatikh L, Swolfs Y. Effect of matrix and fibre type on the impact resistance of woven composites. Compos B Eng 2019:107736. https://doi.org/10.1016/j.compositesb.2019.107736. in submiss.
[38] ASTM. Standard test methods for constituent content of composite materials. ASTM Int 2010;1–6. https://doi.org/10.1520/D3529M-10.2.
[39] ASTM standard. ASTM D 5229– 92 – standard test method for moisture absorption properties and equilibrium conditioning of polymer matrix composite materials. Annu Book ASTM Stand 2010;92:1–13. https://doi.org/10.1520/D5229.
[40] Riccio A, De Luca A, Di Felice G, Caputo F. Modelling the simulation of impact induced damage onset and evolution in composites. Compos B Eng 2014;66:340–7. https://doi.org/10.1016/j.compositesb.2014.05.024.
[41] Burneau A. Near infrared spectroscopic study of the structures of water in proton acceptor solvents. J Mol Liq 1990;46:99–127. https://doi.org/10.1016/0167-7322(90)80048-O.
[42] Krupka J, Gregory AP, Rochard OC, Clarke RN, Riddle B, Baker-Jarvis J. Uncertainty of complex permittivity measurements by split-post dielectric resonator technique. J Eur Ceram Soc 2001;21:2673–6. https://doi.org/10.1016/S0955-2219(01)00343-0.
[43] Idolor O, Guha R, Grace L. A dielectric resonant cavity method for monitoring of damage progression in moisture-contaminated composites. Am. Soc. Compos. 2018;2. https://doi.org/10.12783/asc33/25963. Lancaster, PA: DEStech Publications, Inc.; 2018.
[44] Idolor O, Guha R, Bilich L, Grace L. 2-Dimensional mapping of damage in moisture contaminated polymer composites using dielectric properties. Am. Soc. Compos. 2019. https://doi.org/10.12783/asc34/31312. Lancaster, PA: DEStech Publications, Inc.; 2019.
[45] Bull DJ, Helfen L, Sinclair I, Spearing SM, Baumbach T. A comparison of multi-scale 3D X-ray tomographic inspection techniques for assessing carbon fibre composite impact damage. Compos Sci Technol 2013;75:55–61. https://doi.org/10.1016/j.compscitech.2012.12.006.
[46] Meola C, Carlomagno GM. Non-destructive evaluation (NDE) of aerospace composites: detecting impact damage. https://doi.org/10.1533/9780857093554.3.367; 2013.
[47] Liu J, Koenig L. A new baseline correction algorithm. Using Objective Criteria 1987;41:447–9.
[48] Musto P, Karasz FE, MacKnight WJ. Fourier transform infra-red spectroscopy on the thermo-oxidative degradation of polybenzimidazole and of a polybenzimidazole/polyetherimide blend. Polymer 1993;34:2934–45. https://doi.org/10.1016/0032-3861(93)90618-K.
[49] Sales R, Thim G, Brunelli D. Understanding the water uptake in F-161 glass-epoxy composites using the techniques of luminescence spectroscopy and FT-NIR. Polímeros 2017;27:171–82. https://doi.org/10.1590/0104-1428.05516.
[50] Huo Z, Anandan S, Xu M, Chandrashekhara K. Investigation of three-dimensional moisture diffusion modeling and mechanical degradation of carbon/bismaleimide composites under seawater conditioning. J Compos Mater 2018;52:1339–51. https://doi.org/10.1177/0021998317725159.
[51] Guha RD, Idolor O, Grace L. Molecular dynamics (MD) simulation of a polymer composite matrix with varying degree of moisture: investigation of secondary bonding interactions. Am. Soc. Compos. 2019. https://doi.org/10.12783/asc34/31367. Lancaster, PA: DEStech Publications, Inc.; 2019.
[52] Roqueta G, Fmq Jl. Non-destructive evaluation (NDE) of composites: microwave techniques. Non-destructive eval. Polym. Matrix compos. Elsevier Science & Technology; 2013.
[53] Milosevic M, Berets SL. A review of FT-IR diffuse reflection sampling considerations. Appl Spectrosc Rev 2002;37:347–64. https://doi.org/10.1081/ASR-120016081.
[54] Cole KC, Noël D, Hechler J-J. Applications of diffuse reflectance fourier transform infrared spectroscopy to fiber-reinforced composites. Polym Compos 1988;9:395–403. https://doi.org/10.1002/pc.750090605.
[55] Lin YC, Chen X. Investigation of moisture diffusion in epoxy system: experiments and molecular dynamics simulations. Chem Phys Lett 2005;412:322–6. https://doi.org/10.1016/j.cplett.2005.07.022.
[56] Pethrick RA. Non-destructive evaluation (NDE) of composites: dielectric techniques for testing partially or non-conducting composite materials. Non-Destructive Eval Polym Matrix Compos Tech Appl 2013;2013:116–35. https://doi.org/10.1533/9780857093554.1.116.